Hindawi
Mathematical Problems in Engineering
Volume 2020, Article ID 3074671, 14 pages
https://doi.org/10.1155/2020/3074671

Research Article

Performance Analysis of Hydrodynamic Pressure Finger Seal by Wall Slip Effect

Yan-chao Zhang[1], **Ting Wang**[1], **Dong-ya Zhang**[1], **Ming-hu Yin**[1], **Ya-hui Cui**[1], **Ling-ping Chen**[1], **Peng-fei Du**[2] **and Rui Wang**[3]

[1]*School of Mechanical Instrumental Engineering, Xi'an University of Technology, Xian 710048, China*
[2]*China Aerospace Science and Technology Corporation, Xi'an Aerospace Propulsion Test Technique Institute, Xi'an 710100, China*
[3]*Shaanxi Ruihong Mechanical and Electrical Technology Co., Ltd., Xi'an 710611, China*

Correspondence should be addressed to Yan-chao Zhang; zhangyanchao@xaut.edu.cn

Received 30 December 2019; Revised 11 May 2020; Accepted 3 June 2020; Published 4 July 2020

Academic Editor: Ramon Sancibrian

Hydrodynamic pressure finger seal1 is a kind of flexible noncontact dynamic sealing device with good application potential. It relies on the ultrathin dynamic pressure film effect produced by the rotation of finger boot and rotor to realize the design of noncontact and low leakage and is suitable for high-speed dynamic sealing parts. However, under the high-speed condition, there is a wall slip effect when the gas flows in the microchannel with a thickness of about 10 μm between the finger boot and rotor, which affects the stability of the dynamic pressure air film and also affects the change of the air film bearing capacity and the leakage rate of the finger seal. Therefore, based on the theory of microflow, the interstitial flow field model of finger seal under fluid dynamic pressure is established, and its slip effect under high speed is analyzed. The results show that the slip ratio of the sealing medium temperature of 500°C and 0.1 MPa conditions reached 27.28%. When considering the slip effect of the wall surface generated by the gas under shear driving, the gas film bearing capacity decreased and the leakage rate increased. When the pressure difference between the upper and lower reaches of the seal is 0.1 MPa, and the rotor line speed is 400 m/s, the gas film bearing capacity decreases by 17.39% after considering the slip effect of the wall surface, and the leakage rate increases by 14.06%. The results provide an important reference for the structural design and leakage control of hydrodynamic finger seal.

1. Introduction

The hydrodynamic pressure finger seal is a new type of finger seal derived from the contact finger seal; meanwhile, the characteristic of low leakage of contact finger seal and long life of noncontact seal are also made [1, 2]. Due to its characteristics of good sealing performance and low manufacturing cost, it has a wide application prospect in improving the performance of aero-engine [3].

In view of the excellent application prospect of hydrodynamic finger seal, many researchers have carried out a lot of research on fluid dynamic pressure finger, the effect of the stiffness of finger beam, the stiffness of air film, and the bearing capacity seal. By using finite element simulation and equivalent dynamic model, Marie [4] studied air film on the sealing performance of hydrodynamic finger seal and also analyzed the displacement transfer rate of hydrodynamic air film, providing an important idea for the theoretical design and study of hydrodynamic finger seal.

According to the temperature characteristic, such as hydrodynamic pressure under the effect of dynamic characteristics. Braun et al. [5] analyzed the thermal characteristics of hydrodynamic pressure of finger seal, finite element analysis method to analyze the different rotating speed and sealing medium environment temperature, hydrodynamic pressure finger seal leakage flow characteristics, and the method of equivalent dynamic hydrodynamic finger seal dynamic characteristics. For the hydrodynamic pressure of finger seal

structure design, selection of materials and the temperature rising characteristic research provides an important reference. Temis et al. [6] also studied the adaptability of hydrodynamic finger seal to the dynamic adjustment of rotor by using fluid-solid coupling simulation method and equivalent method and studied the feasibility of the formation of dynamic pressure air film. Fleming [7] conducted a study on the effect of rotating speed and film thickness on the sealing performance of hydrodynamic finger seal and confirmed that the fluid film always exists in various operating conditions. Proctor et al. [8] studied the leakage, power consumption, and wear characteristics of hydrodynamic finger seal under static conditions and fixed linear velocity under the condition of 56.7 m/s by using the upstream and downstream pressure difference and conducted comparative analysis with brush seal and contact finger seal. Meanwhile, the structural design, theoretical analysis of dynamic characteristics, and performance simulation research in combination with the working characteristics of the hydrodynamic finger seal were also carried out [9–15].

At present, the research on hydrodynamic finger seal mainly focuses on the design of the finger beam line [16], the optimization of the axial structure of the finger seal [17], the construction of the equivalent dynamic model of the finger seal, and performance simulation analysis [18]. However, the study of hydrodynamic pressure finger seal leakage flow characteristics still needs to be further explored. Due to the slip phenomenon of the wall surface during the flow of gas in the microchannel with a thickness of about 10 μm between the finger boots and the rotor, the slip effect of gas flow in the microchannel was not considered in previous studies, and this microscale flow slippage phenomenon has an important influence on the parameters such as gas film bearing capacity and leakage rate of hydrodynamic pressure finger seal [19]. Therefore, the analysis of leakage gap flow field characteristics of hydrodynamic finger seal, considering the wall slip effect on leakage flow, can enrich the design and engineering application of high-performance hydrodynamic finger seal and is of great significance for the improvement of aero-engine sealing technology.

Therefore, based on the microscale flow theory, a flow field model of hydrodynamic pressure finger seal leakage gap is established, and the flow slip characteristics of the microscale leakage channel seal medium are studied. In this paper, by simulating the flow state of the gas under the condition of wall slip, the difference between the gas film bearing capacity and the leakage volume under the condition of considering wall slip at a specific speed and the boundary condition without wall slip is analyzed, and the flow of the sealing medium in the leakage gap flow field driven by shear is simulated numerically. It provides theoretical guidance for calculating leakage performance of hydrodynamic finger seal under dynamic conditions and verifying the rationality of test results.

2. Hydrodynamic Pressure Finger Seal Structure Characteristics and Working Principles

The hydrodynamic finger seal consists of high-pressure finger plates, low-pressure finger plates with sealing boots, front and rear baffles, rivets, and other components, and its structure is shown in Figure 1. Different from the contact finger seal, the seal boot at the free end of the low-pressure finger plate adds an extended lengthening structure in the axial direction. When the rotor rotates at high speed, an action pressure film is formed between the low-pressure sealing boots and the rotor, and the low-pressure sealing boots are lifted to achieve noncontact between the seal and the rotor. At the same time, the action pressure film hinders the leakage of the seal medium in the leakage gap. The fluid dynamic pressure film formed by the rotor rotation can ensure the seal's low leakage and long-life characteristics, and the flexible finger beam sealed by the fluid dynamic pressure finger can adapt to the radial dynamic beating caused by the rotor due to vibration or thermal deformation. Therefore, this hydrodynamic pressure finger seal is suitable for dynamic sealing conditions with demanding seal leakage level and high work life requirements, which makes it have good working performance and application prospects.

3. Hydrodynamic Pressure Finger Seal Slip Effect

3.1. Leakage Flow Analysis of Hydrodynamic Pressure Finger Seal. The sealing function of hydrodynamic pressure finger seal is mainly based on the action of the dynamic pressure gas film formed between the low-pressure seal boot and the rotor. Under high-speed conditions, the thickness of the gas film is only about 10 μm, and macroscopic fluid mechanics models and formulas may no longer be suitable for microscale flow. Since the characteristic scale of flow field is reduced to micron level, the flow characteristics of fluid show significant size effect compared with macroscopically. At this point, many physical quantities in the macroscopic state will change, and the flow speed on the surface of the channel will show a slip phenomenon, and the surface viscous shear stress will be reduced accordingly. At this point, the effect of the wall slip on the flow of gas sealed by the hydrodynamic pressure finger cannot be ignored. For this reason, the study refers to the study of wall velocity slip under the micronanometer gap flow field at home and abroad. Considering the influence of wall velocity slip, the leakage flow analysis of hydrodynamic pressure finger seal is presented [20, 21].

In the microscale gas flow, K_n (Knudsen) number is usually used to describe the degree of microscaling of the flow. K_n number is a dimensionless number. Like the Re number and the M number, it has a very important position in the study of gas flow [22], and K_n is calculated in the following equation:

$$K_n = \frac{\lambda}{L}, \tag{1}$$

where λ is the mean molecular free path of the gas and L is the characteristic scale of the flow field. According to the size of K_n number, the gas flow field can be divided as follows:

(1) When $K_n \le 10^{-3}$, this field of flow belongs to the continuous medium area. Fluid motion can be simulated using the N–S equation plus nonslip boundary conditions. (2) When $10^{-3} < K_n \le 10^{-1}$, this field of flow belongs to the

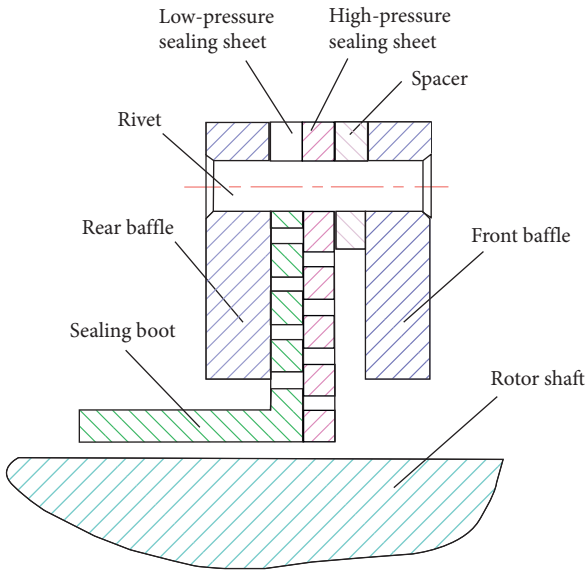

Figure 1: Structure of hydrodynamic finger seal.

slip area. The fluid begins to deviate from the thermodynamic equilibrium, at which point the fluid can still be described by the N–S equation, but the boundary slip conditions need to be revised. (3) When $10^{-1} < K_n \leq 10$, this field of flow belongs to the transition area. At present, the flow problem in this research area is usually solved by Boltzmann equation, Monte Carlo method, and other methods. (4) When $K_n > 10$, this field of flow belongs to the molecular free flow area. In the free molecular zone, air flow is usually described and analyzed using the point of view of particle motion.

Combined with the actual working conditions of the hydrodynamic pressure finger seal, the minimum characteristic scale of the flow field is 0.00635 mm, and the average free path calculation of the gas molecule is shown in the following formula:

$$\overline{\lambda} = \frac{1}{\sqrt{2}\pi d^2 n}, \tag{2}$$

where d represents the diameter of the gas molecule and n represents the density of the number of molecules.

According to Boltzmann's theory, the ideal gas state equation for the sealed medium in the leakage gap can be constructed as shown in the following:

$$P = nkT, \tag{3}$$

where P represents the working pressure of the gas. In this article, the actual working pressure is 0.1×10^6 Pa, k represents the Boltzmann constant, and $k = 1.3806505 \times 10^{-23}$ J/K.

Formula (3) is brought into formula (2), and the average free path calculation formula (4) of the gas molecule is reduced:

$$\overline{\lambda} = \frac{kT}{\sqrt{2}\pi d^2 P}. \tag{4}$$

According to the actual operating state of fluid dynamic pressure, the temperature $T = 773$ K and the air molecular diameter $d = 3.46 \times 10^{-10}$ m are taken. According to formula (4), the average free path of the gas molecule is calculated to be $\lambda = 2.0065 \times 10^{-7}$ m.

According to the K_n value calculation formula (1), $K_n = 0.03159$ is obtained. Obviously, $10^{-3} < K_n \leq 10^{-1}$, so it can be seen that the range of K_n number is in the slip region. At this point, although the collision frequency between gas molecules is still much higher than the collision frequency between gas molecules and solid wall surfaces, the microscale effect cannot be ignored. In the slip zone, the thin effect gradually begins to appear, and the fluid begins to deviate from the thermodynamic equilibrium. At this time, the fluid can still be described by the N–S equation, but the boundary slip conditions need to be revised.

By analyzing the characteristics of the watersheds in the hydrodynamic pressure finger seal leak channel, it is shown that the boundary condition of the nonslip wall surface may no longer be applicable to the calculation when the gas flows in the hydrodynamic pressure finger seal tiny leakage channel. At the same time, the slip effect of the wall surface at the microscale downstream solid coupling interface is verified. The slip boundary condition of the wall surface becomes an unnegligible factor affecting the leakage flow characteristics, which affects the overall working stability and reliability of the hydrodynamic pressure finger seal system. This effect is particularly important for the clearance flow under extreme conditions such as high shear and heavy loads.

3.2. Slip Effect of Hydrodynamic Finger Seal. For the slip law of the wall, Navier first proposed the simple slip model formula (5) and considered the velocity of the fluid medium near the wall as a simple function of the velocity gradient, as shown in the following:

$$u_{\text{slip}} = \beta\left(\frac{\partial u}{\partial n}\right)_w. \tag{5}$$

In the abovementioned formula, w represents the wall boundary, β represents the slip length parameter, and u_{slip} represents the wall slip speed. Since then, the slip boundary condition model of the wall surface has been called the Navier slip model. The Navier slip model has been validated by experiments and molecular dynamics simulations and has been used in research to consider the slip phenomenon of the wall surface. However, when applying the Navier slip model, there is no strict distinction between liquid and gas.

For the gas slip law, Maxwell proposed the slip equation (6) for thin gas kinematics:

$$u_{\text{slip}} = \frac{2-\delta}{\delta}\lambda\left(\frac{\partial u}{\partial n}\right)_w, \tag{6}$$

where δ is the interface momentum adjustment coefficient, which represents the ratio of the number of molecules reflected by the gas molecule at the solid wall surface, and λ represents the average free path of the gas molecule. The

Maxwell slip model formula is the slip condition of the wall surface of the gas. The slip model of the gas is often used in ultra-high-speed microscale analysis.

Because the rotor moves at speed v relative to the sealing boot, the sealed boot is fixed, and the motion of the rotor drives the flow of gas. Therefore, the established shear flow model is shown in Figure 2.

From the N–S equation, it can be obtained that the control equation is

$$\frac{\mathrm{d}p}{\mathrm{d}x} = \mu \frac{\mathrm{d}^2 u}{\mathrm{d}y^2}. \tag{7}$$

In the above equation, u is the velocity component of the rotor that drives the gas, μ is the hydrodynamic viscosity, and the pressure gradient $\mathrm{d}p/\mathrm{d}x$ is the constant value.

Integration of equation (7) can be obtained as follows:

$$\frac{\mathrm{d}u}{\mathrm{d}y} = \frac{y}{\mu}\frac{\mathrm{d}p}{\mathrm{d}x} + c_1, \tag{8}$$

$$u = \frac{y^2}{2\mu}\frac{\mathrm{d}p}{\mathrm{d}x} + c_1 y + c_2. \tag{9}$$

Considering the slip boundary conditions on the wall, the boundary conditions in formulae (8) and (9) are shown in the following formula:

$$\begin{cases} y = 0, \quad u = L_s \dfrac{\mathrm{d}u}{\mathrm{d}y}, \\ y = h, \quad u = V - L_s \dfrac{\mathrm{d}u}{\mathrm{d}y}, \end{cases} \tag{10}$$

where L_s represents the slip length of the fluid in the gap and can be obtained from the following:

$$L_s = \frac{2-\delta}{\delta}\lambda, \tag{11}$$

where δ is the interface momentum adjustment coefficient, which represents the proportion of molecules reflected by gas molecules at the solid wall surface. In general, the value range is 0.1 to 0.2 and here is 0.1 computation [23, 24]. λ represents the average free path of gas molecules.

Bringing the boundary conditional formula (10) into equations (8) and (9), the integral constants c_1, c_2 calculations can be obtained as shown in the following:

$$c_1 = \frac{1}{h + 2L_s}\left(V - \frac{h^2}{2\mu}\frac{\mathrm{d}p}{\mathrm{d}x}\right), \tag{12}$$

$$c_2 = \frac{L_s}{h + 2L_s}\left(V - \frac{h^2}{2\mu}\frac{\mathrm{d}p}{\mathrm{d}x}\right). \tag{13}$$

The slip velocity formula (14) can be obtained by bringing the obtained integral constants c_1, c_2 into equation (9):

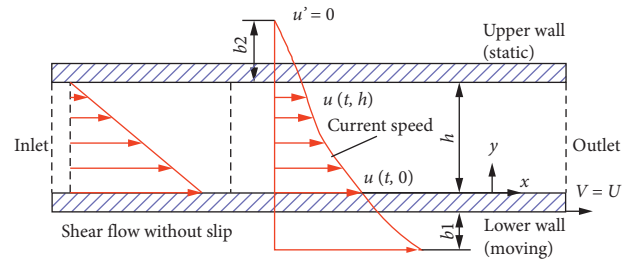

Figure 2: Shear flow model.

$$u = \frac{h^2}{2\mu}\frac{\mathrm{d}p}{\mathrm{d}x} + \frac{h}{h + 2L_s}V - \frac{(1/2\mu)h^3}{h + 2L_s}\frac{\mathrm{d}p}{\mathrm{d}x} + \frac{L_s}{h + 2L_s}V - \frac{(1/2\mu)L_s h^2}{h + 2L_s}\frac{\mathrm{d}p}{\mathrm{d}x}. \tag{14}$$

When the flow is only caused by the rotation of the rotor, the pressure gradient $\mathrm{d}p/\mathrm{d}x$ is zero in the channel which simplifies as follows:

$$u = \frac{h}{h + 2L_s}V + \frac{L_s}{h + 2L_s}V = \frac{h + L_s}{h + 2L_s}V. \tag{15}$$

The slip speed of the rotor and the rotor speed in the channel are shown in the following:

$$\frac{u}{V} = \frac{h + L_s}{h + 2L_s} = 1 - \frac{L_s}{h + 2L_s}, \tag{16}$$

where h is the clearance height and L_s is the slip length parameter.

According to the slip model equation of the Navier wall surface and the slip equation of the thin gas kinematics proposed by Maxwell, the slip parameter L_s can be obtained. Based on the above calculation, the average free path of the gas molecule is $\lambda = 2.0065 \times 10^{-7}$ m. The slip parameter $L_s = 3.81235 \times 10^{-6}$ m. The ratio of rotor slip speed and rotor speed in the channel is 0.7272.

The slip rate can be obtained according to the slip rate formula:

$$S = \frac{V_w - V_f}{V_w}, \tag{17}$$

where V_w is the wall rotor speed, and V_f is the speed at which the wall surface drives the gas molecules in the gap flow field. The slip rate can be calculated as $s = 27.28\%$.

The calculated slip rate can be used as the boundary condition for hydrodynamic pressure finger seal leakage calculation.

4. Simulation Models and Methods

4.1. Calculation Model of Hydrodynamic Finger Seal. Hydrodynamic pressure finger seal leakage performance analysis is realized by analyzing the fluid region between finger seal and seal rotor. Considering that hydrodynamic

pressure finger seal has cyclic symmetry characteristics on the structure, in the analysis model, only one cyclic unit was selected, and the leakage gap between the high-pressure and low-pressure finger boots and the rotor was used as the fluid analysis area to reduce the calculation amount. The region of the fluid is shown in Figure 3.

The hydrodynamic pressure finger seal is made up of two interlaced pieces of low-pressure finger and high-pressure finger. As shown in Figure 4, for the intuitive display, a distance is drawn between the two. Among them, the gap between the two high-pressure finger beams in the high-pressure seal sheet and the three areas of the two cuneiform gas membranes between the high-pressure finger boots and the external surface of the rotor constitute the first half of the flow domain. The two gaps formed between a finger beam in a low-pressure finger seal and a finger beam in the front and rear, and the cuneiform gas membrane between the low-pressure finger boot and the outer surface of the rotor constitutes the latter half of the flow domain. Therefore, the stream domain can be divided into six parts. The hydrodynamic pressure finger seal flow area calculation model is shown in Figure 4, and the corresponding finger seal structure parameters are shown in Table 1.

The simulation analysis is completed through the Ansys Workbench 15.0 CFX (Computational Fluid Dynamics X) fluid analysis module. The inlet of the air flow between the high-pressure boots and the rotor in figure *b* is set as the open boundary condition of Opening 1. According to the pressure of sealing medium, it is set as the pressure boundary condition. In the figure, the two-way straight arrow indicates that airflow can be in or out. The central region is the upper surface of the airflow layer between high- and low-pressure boots and rotor, and it is the interface surface of fluid-solid coupling, which is set as interface boundary condition. The inner area is the outlet of airflow, and the open boundary condition is set as Opening 2. The pressure boundary condition is given according to the pressure of the leaking low-pressure chamber. The area on both sides is set as the boundary condition of symmetry, which is the circumferential circular symmetrical wall surface of leakage clearance. The lower surface of the air layer between the high and low-pressure boots and the rotor is in contact with the rotor, which is set as the condition of moving wall, and the moving speed takes into account the effect of slip rate.

4.2. Analysis of Grid Independence. In order to eliminate the influence of mesh quality on the calculation results and reduce the calculation time and complexity, this paper analyzes the mesh quality independence of hydrodynamic pressure finger seal fluid structure coupling. The number of meshes can be controlled by adjusting the related parameters such as element sizing and relation. Taking the number of grids in solid domain and fluid domain as variables and the leakage amount of hydrodynamic finger seal as analysis target, the influence of different grid numbers on the leakage amount is analyzed comparatively.

As shown in Figure 5, when the number of grids in solid domain and fluid domain is lower than a certain value, the leakage corresponding to different number of grids varies greatly. When the total number of grids is 51600, the leakage is 2.62×10^{-5} kg/s. When the number of meshes exceeds this value, with the increase of the number of meshes, the change of leakage value is very small. Therefore, as long as the number of selected grids exceeds the above values, the calculation results are independent of the grid. Figure 6 shows the grid under the current settings.

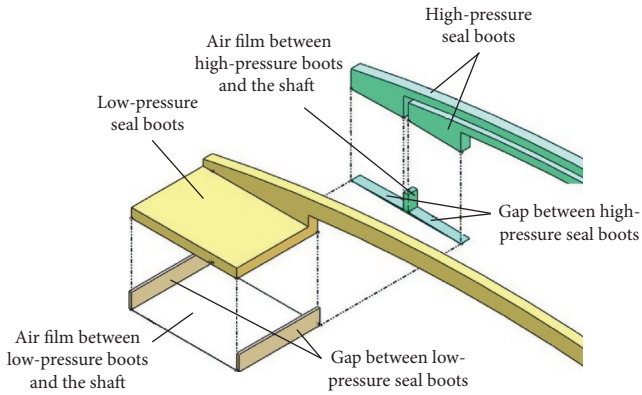

Figure 3: Hydrodynamic pressure finger seal fluid region composition.

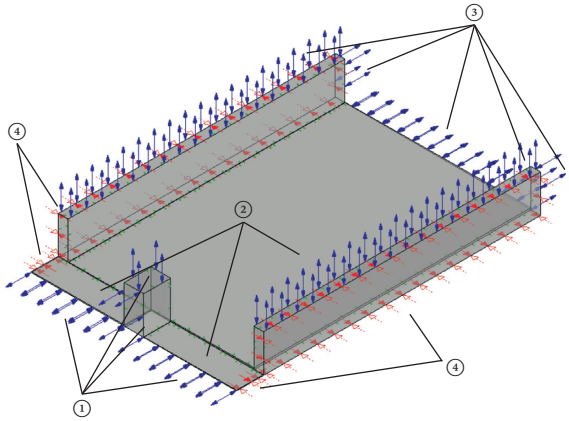

Figure 4: Flow field calculation model of hydrodynamic finger seal.

Table 1: Structural parameters of hydrodynamic pressure finger seal.

Parameter	Value
Finger seal outer diameter (mm)	100
Finger seal internal diameter (mm)	66.04
Finger beam root circle diameter (mm)	84
Number of finger seal beams	48
Rotor radius (mm)	66
Boot height (mm)	0.5
Thickness of the finger seal sheet (mm)	0.3
Minimum air film gap (mm)	0.00635
Circumferential thickness ratio of gas film	3.15

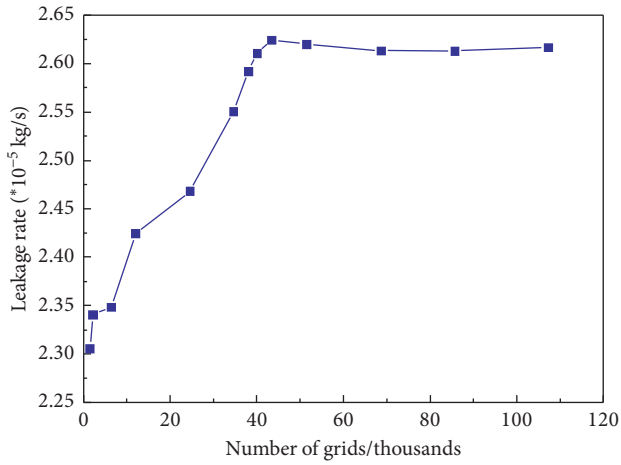

Figure 5: Analysis of mesh quality independence.

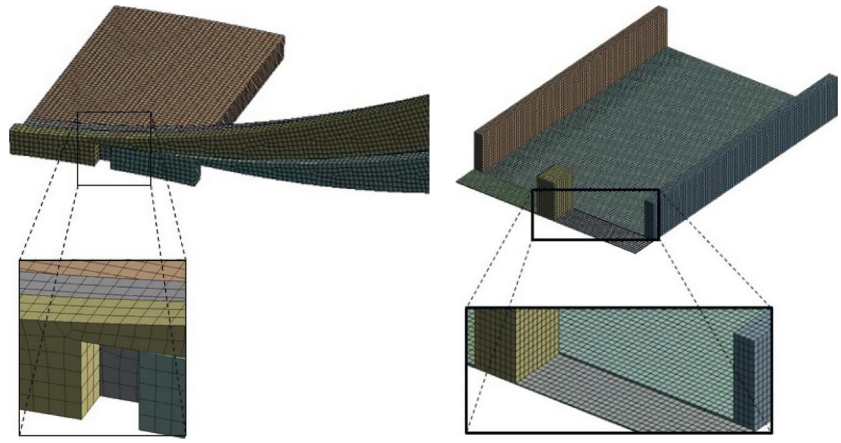

Figure 6: Grid partitioning. (a) Grid division of solid domain. (b) Grid division of fluid domain.

4.3. Verification of the Simulation Method. In [25], the noncontact finger seal with herringbone groove structure on the rotor surface has been tested in a very tight dynamic and static state, and the detailed and credible test data are given. In order to verify the accuracy of the numerical model in this paper, the same numerical model as that in [25] is established, and the two-way fluid structure coupling calculation is carried out under the same boundary conditions as the experimental values. Finally, the calculation results are compared with the test data.

The leakage characteristic test parameters in [25] are given in the form of flow factors, which are defined as follows:

$$\phi = \frac{\dot{m}\sqrt{T_{\text{avg}}}}{P_u \times D_{\text{seal}}}, \tag{18}$$

where $\dot{m}$ is the mass flow through the whole flow field and the unit of it is kg/s; T_{avg} is the average temperature of the finger seal inlet and the unit of it is k; P_u is the finger seal inlet pressure and the unit of it is MPa; D_{seal} is the outer diameter of the rotor corresponding to the finger seal and the unit of it is m. Therefore, the unit of flow factor is kg·K$^{1/2}$/(MPa·m·s). In this paper, a group of dynamic test data is selected to compare with the numerical simulation results, as shown in Figure 7. When the temperature is 300 K and the rotating speed is 5000 r/min and the pressure difference is 13.8 kPa, 34 kPa, 69 kPa, 103 kPa, 138 kPa, 176 kPa, 207 kPa, and 241 kPa, respectively, the flow factors calculated by simulation are consistent with the overall trend of the test results in [25].

It can be seen from Figure 7 that when the pressure difference is 103 kPa, the change rate of flow factor is large, and the curve begins to become gentle and gradually keeps consistent with the change rate of simulation results. This is due to the uncontrollable factors such as assembly state and leakage channel in the test, which lead to the difference between the initial low-pressure difference and the high-pressure difference. When the pressure difference exceeds 69 kPa, the simulation result is smaller than the test result. The reason analysis is as follows. First, the leakage in the

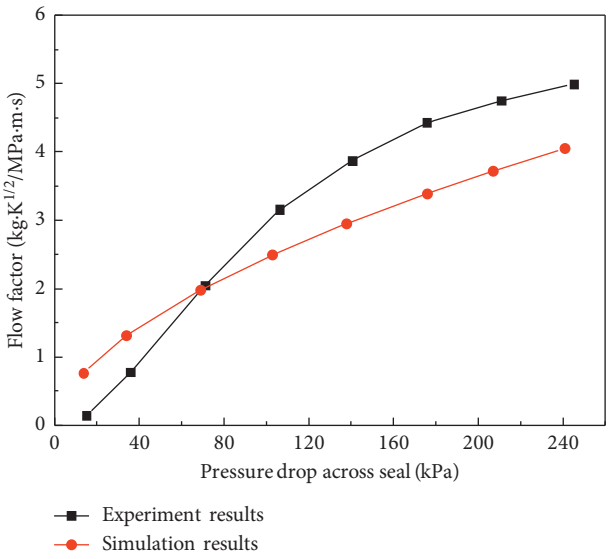

Figure 7: Comparison of simulation and test results.

actual test includes three channels, and the simulation model mainly considers two channels: finger boot gap and finger gap leakage. Second, the leakage caused by temperature effect, rotor vibration, and other uncontrollable factors will increase in the test process. The simulation value is about 80% of the test value, which is also consistent with the previous saying that the leakage path of finger seal is mainly the leakage between finger boots and finger pieces, thus verifying the accuracy and reliability of the numerical method and simulation model.

5. Results and Discussion

When the pressure difference in the upper and lower reaches of the seal is 0.1 MPa, the ambient temperature is 500°C, and the rotor surface line speeds v are 100 m/s, 200 m/s, 300 m/s, and 400 m/s, respectively, the slip effect of the wall surface is considered, and the simulation analysis is passed. Hydrodynamic pressure finger seal leaks within the same channel pressure distribution cloud diagram as shown in Figure 8, and seal medium leakage flow cloud diagram is shown in Figure 9.

In Figures 8(a), 8(c), 8(e), and 8(g), we have rotor surface line speeds of 100 m/s, 200 m/s, 300 m/s, and 400 m/s, regardless of the results of the simulation of the flow pressure of the sealed medium during the slip of the wall surface. Figures 8(b), 8(d), 8(f), and 8(h) are the pressure cloud images of the simulation results of sealing medium flow under the same working conditions when the slip effect of the wall surface is considered. As can be seen from Figure 8, considering slippage has a significant impact on the results of the analysis. When the rotor speeds are 100 m/s, 200 m/s, 300 m/s, and 400 m/s, after counting the wall slip effect, the maximum pressure in the leak channel decreased by 0.011 MPa, 0.046 MPa, 0.107 MPa, and 0.232 MPa, respectively. The reason is that when considering the slip effect of the wall surface, the contact surface of the rotor and the sealed medium in the leakage channel appears to slide relatively, and the fluid is no longer consistent with the rotor surface speed under the adhesion force, and the speed is reduced. This is not conducive to the formation of fluid dynamic pressure film between the finger boots and the rotor, resulting in a decrease in the pressure in the leakage gap channel, and with the increase of speed, this change trend is more and more obvious.

Figures 9(a), 9(c), 9(e), and 9(g) shows that when the pressure difference between the upper and lower reaches of the seal is 0.1 MPa, the ambient temperature is 500°C, and the rotor surface line speeds are 100 m/s, 200 m/s, 300 m/s, and 400 m/s. Regardless of the calculation results of velocity field streamline distribution of the sealing medium that avoids slippage, Figures 9(b), 9(d), 9(f), and 9(h) calculated results of leakage velocity field streamline distribution when the wall slip effect is considered. As can be seen from Figure 9, the sealing medium flows from the end of the high-pressure cavity into the leakage channel and flows out from the end of the low-pressure finger boot. As the speed of the rotor surface line increases, the streamline direction gradually tends to level. This is due to the effect of the upstream and downstream pressure differences. Under the action, the seal medium flows from the high-pressure cavity to the low-pressure cavity along the leakage channel. Under the influence of the rotor's circumferential high-speed rotation effect, the leakage fluid is affected by the circumferential shear flow effect due to the presence of the adhesive force of the seal medium, and the higher the speed, the more obvious the effect. Therefore, it shows that the downstream streamline tends to level under the condition of ultra-high speed; that is, it tends to be consistent with the circular motion of the rotor.

The velocity field calculation in Figure 9 also shows that when the rotor surface line speeds are 100 m/s, 200 m/s, 300 m/s, and 400 m/s, after considering the wall slip effect, the maximum velocity of the sealing medium in the circumferential leakage flow is reduced by 1.8 m/s, 40.1 m/s, 81.8 m/s, and 109.1 m/s. This is because the circumferential velocity of the sealing medium is related to the formation of the dynamic air film in the leakage gap. The greater the circumferential speed, the better the dynamic pressure effect. Therefore, considering the slip of the wall surface, because the speed of the sealing medium along the circumferential motion decreases, it is not conducive to the formation of dynamic pressure gas film, which reduces the sealing effect. This is also very consistent with the stress reduction in Figure 8.

In order to analyze the influence of slippage on the sealing performance of hydrodynamic finger under different pressure differences, the change of sealing medium in the leakage channel of hydrodynamic finger seal was studied by simulation analysis when the temperature was 500°C, and the upstream and downstream pressure differences were 0.1 MPa, 0.2 MPa, and 0.3 MPa, respectively. As shown in Table 2, the value of slip ratio under different pressure difference conditions is calculated by theoretical formula. Figures 10 and 11 are the simulation results of gas film bearing capacity and leakage rate of hydrodynamic finger seal under different rotating speed and pressure difference conditions, respectively.

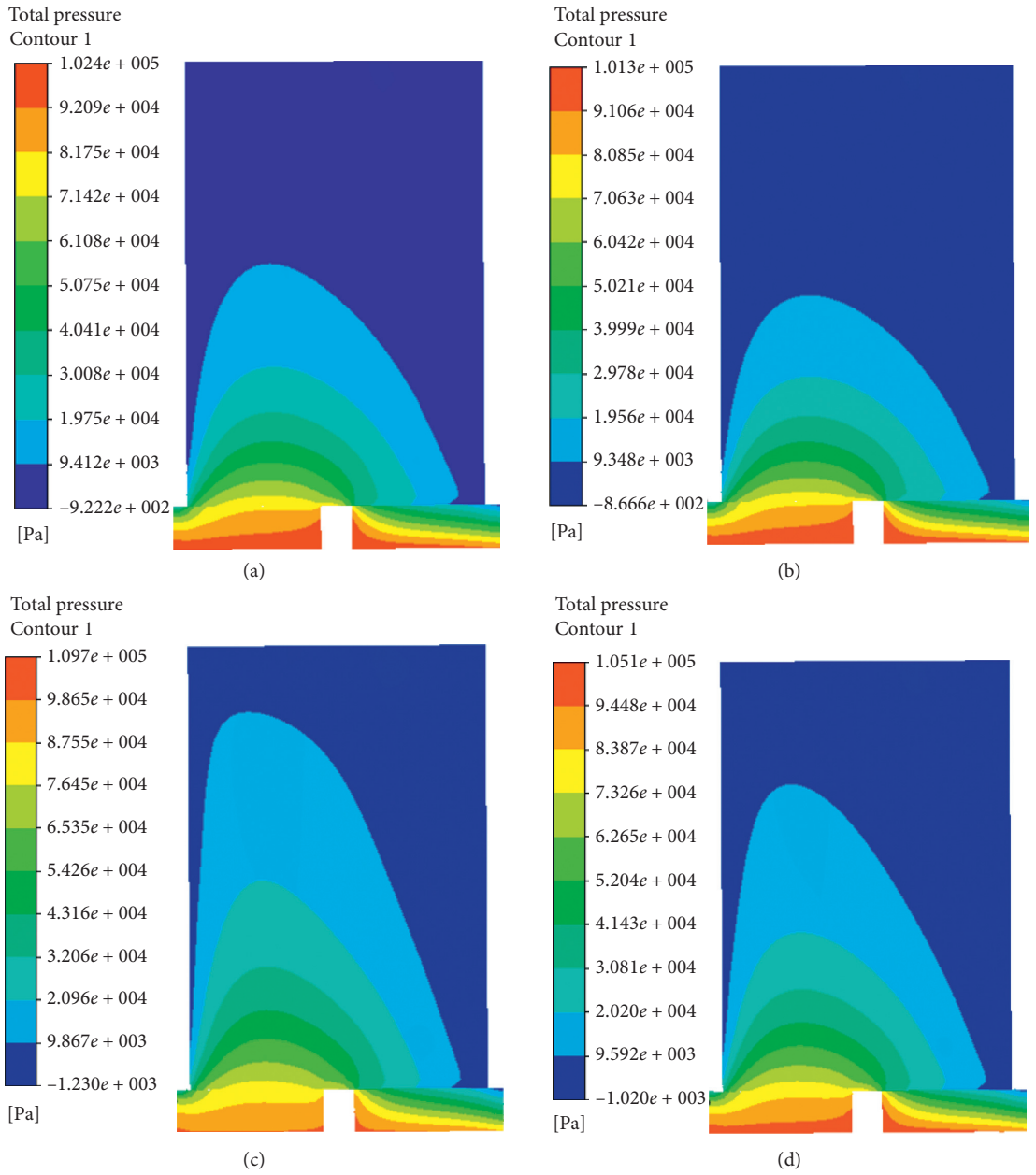

Figure 8: Continued.

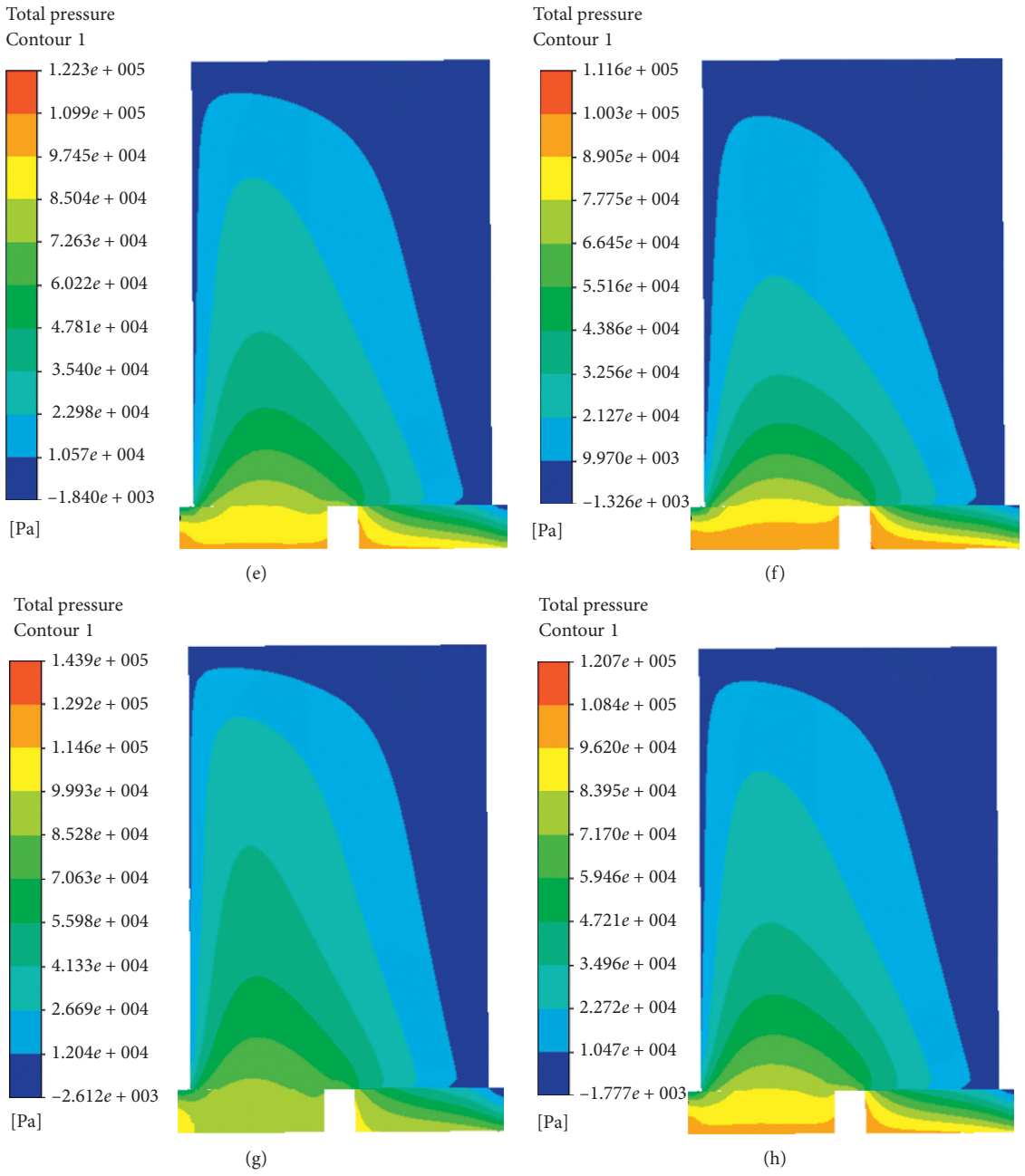

Figure 8: Pressure calculation results in the leakage channel. (a) No slip ($v = 100$ m/s). (b) Slip ($v = 100$ m/s). (c) No slip ($v = 200$ m/s). (d) Slip ($v = 200$ m/s). (e) No slip ($v = 300$ m/s). (f) Slip ($v = 300$ m/s). (g) No slip ($v = 400$ m/s). (h) Slip ($v = 400$ m/s).

As can be seen from Figure 10, when the rotor line speed is fixed, the bearing capacity of the air film shows a gradual increase with the increase of the pressure difference between the upper and lower reaches of the seal. However, compared with the slip of the wall surface, considering the slip, the bearing capacity of the dynamic pressure film in the leakage gap appears to decrease, and this trend is more obvious with the increase of rotor surface line speed and upstream and downstream pressure difference. It can be seen that when the pressure difference between the upper and lower reaches of the seal is 0.1 MPa and the rotor line speeds are 100 m/s, 200 m/s, 300 m/s, and 400 m/s. Taking into account the displacement slip rate of the leakage channel, the bearing capacity of the gas film was reduced by 5.81%, 10.71%, 14.78%, and 17.39%, and the reduction was reduced as the pressure difference between the upper and lower reaches of the seal increased. The decreases were 1.45%, 2.79%, 3.76%, and 6.49%, respectively, when the pressure difference between the upper and lower reaches of the seal was 0.3 MPa. This phenomenon shows that the higher the rotor speed, the more obvious the wall slip effect of the sealing medium in the microleakage channel and the more obvious the effect of the hydrodynamic finger seal performance on the wall slip under the pressure difference conditions of the same seal. However,

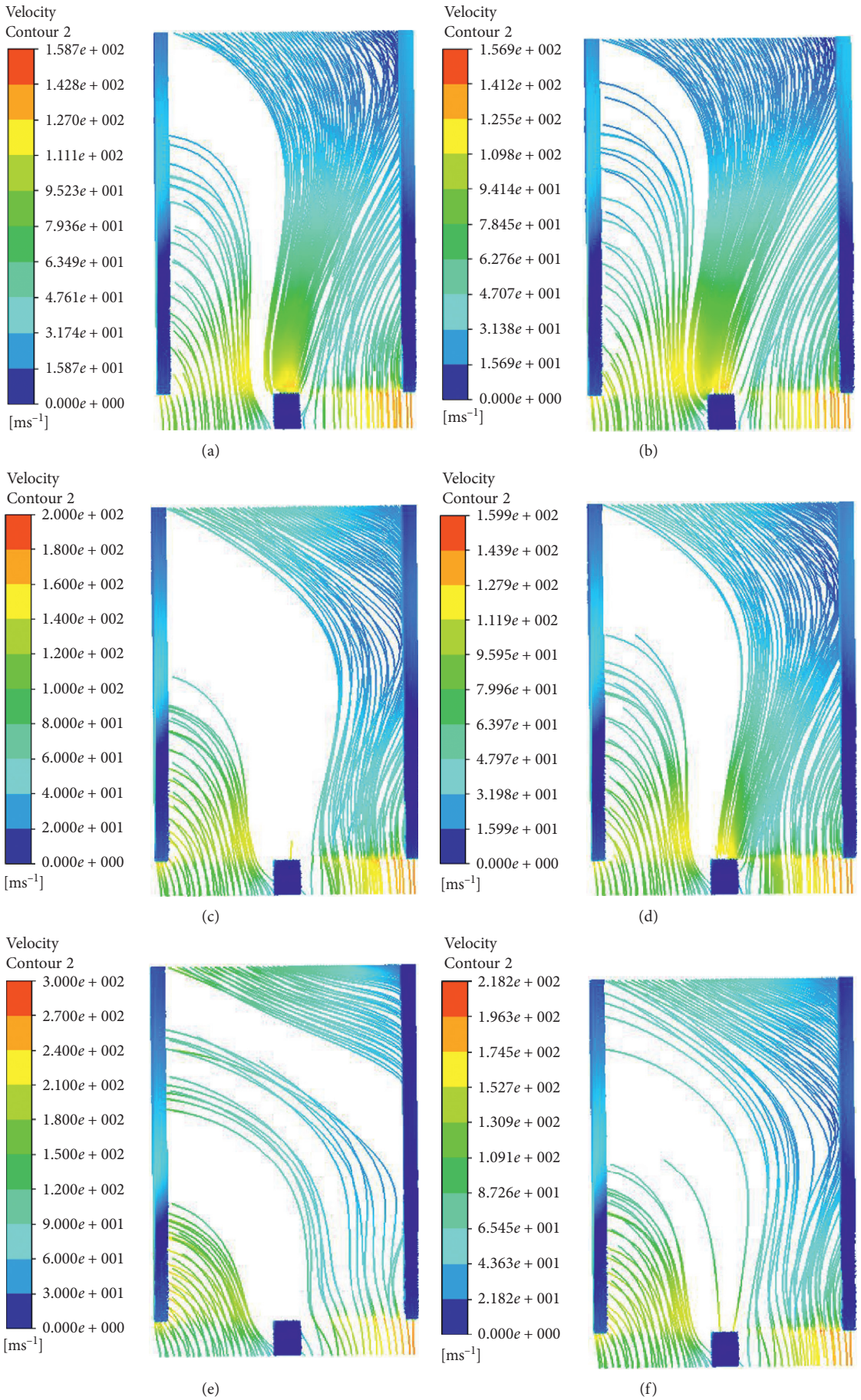

Figure 9: Continued.

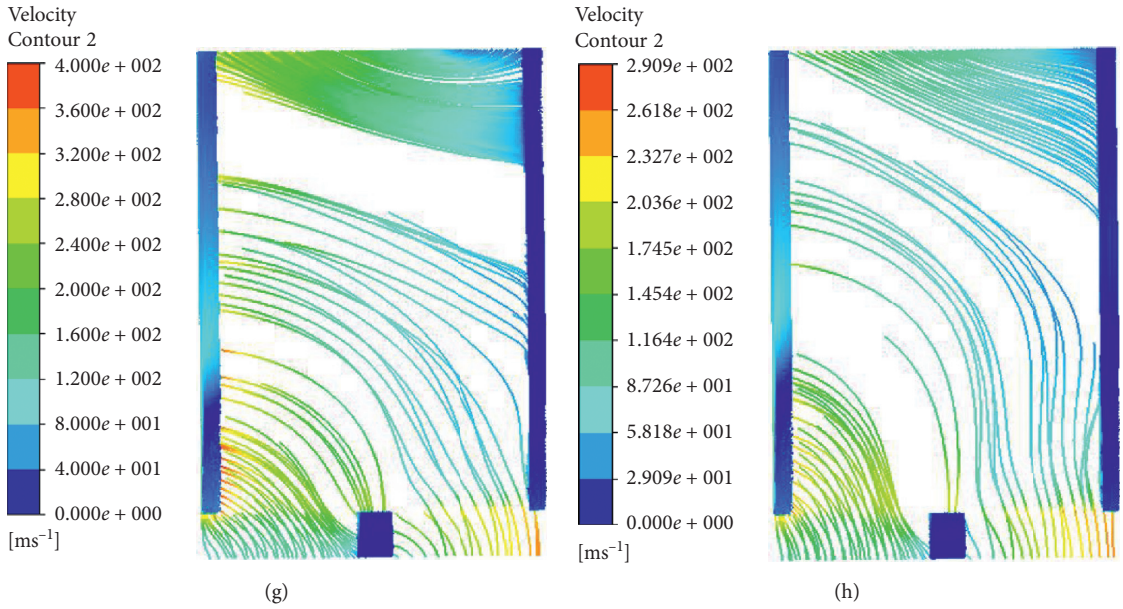

(g) (h)

Figure 9: Calculation results of velocity field in the leakage channel. (a) Velocity streamline with no slip ($v = 100$ m/s). (b) Velocity streamline with wall slip ($v = 100$ m/s). (c) Velocity streamline with no slip ($v = 200$ m/s). (d) Velocity streamline with wall slip ($v = 200$ m/s). (e) Velocity streamline with no slip ($v = 300$ m/s). (g) Velocity streamline with no slip ($v = 400$ m/s). (f) Velocity streamline with wall slip ($v = 300$ m/s). (h) Velocity streamline with wall slip ($v = 400$ m/s).

Table 2: The slip rate under different pressure difference ($T = 500^{\circ}$C).

Pressure difference	0.1 MPa (%)	0.2 MPa (%)	0.3 MPa (%)
Slip rate	27.28	18.76	14.29

it also shows that the effect of pressure flow effect exceeds that of shear flow effect when the pressure difference between the upper and lower reaches of the hydrodynamic finger seal increases to a certain value. Therefore, when the hydrodynamic finger seal is applied to the low-pressure differential high speed, the impact of the wall slip in the design cannot be ignored. When the pressure difference between the upper and lower reaches of the seal increases to a certain extent, the impact of the slip effect can be considered according to the comprehensive impact.

It can be seen from Figure 11 that the leakage rate of the hydrodynamic finger seal decreases gradually with the increase of the speed and increases gradually with the increase of the pressure difference between the upper and lower reaches of the seal. This is due to the pressure flow effect and shear flow effect, and the reason is obvious. At the same time, the results also show that the leakage rate of hydrodynamic pressure finger seal increases under the same working conditions compared with the calculation results without considering the slip conditions of the wall surface. And this trend is more significant with the increase of rotor surface line speed. It can be seen from the figure that, under the pressure 0.1 MPa and the maximum speed of 400 m/s, the leakage of the hydrodynamic finger seal increased by 14.06% as considering the slip conditions of the wall surface. In addition, under the same speed conditions, the pressure difference between the upper and lower reaches of the seal is 0.2 MPa and 0.3 MPa, and the leakage volume increases by 4.78% and 3.92%, respectively, which is consistent with the analysis results of the gas film bearing capacity, and it confirms that the low-pressure difference is high under the conditions of rotation speed. Thus, it is necessary to consider the slip effect of the wall in the design of hydrodynamic finger seal.

The simulation results show that the film bearing capacity is decreased to the maximum value while leakage rate is increased to the maximum at the speed of 400 m/s and pressure of 0.1 MPa. In order to further study and analyze the effect of wall slip on sealing performance at different temperatures, Figures 12 and 13 give the variation of film bearing capacity and leakage rate under typical temperature conditions.

It can be seen from Figure 12 that the gas film bearing capacity shows a trend of decreasing and increasing with the increase of temperature, and the change trend of slip or not considering the wall surface shows the same, and 200°C is the turning point of the change trend. The results also show that the film bearing capacity decreases by more than 12.51% when slip on the wall is considered, and the maximum difference reaches 17.39% at 500°C as the temperature increases.

The results of the calculation in Figure 13 show that, with the increase of temperature, the leakage rate of the wall surface considering the slip or not shows an increasing trend, but considering the slip ratio of the wall surface, the leakage rate is higher than considering the slip of the wall surface. The difference between the wall slip and no wall slip also shows a tendency to reduce first and then increase, and the increase in the value of 500°C reached a maximum of 14.06%, which is related to the reduction in the bearing capacity of the gas film after the slip of the wall and the change in the size of the leakage channel. The results of the

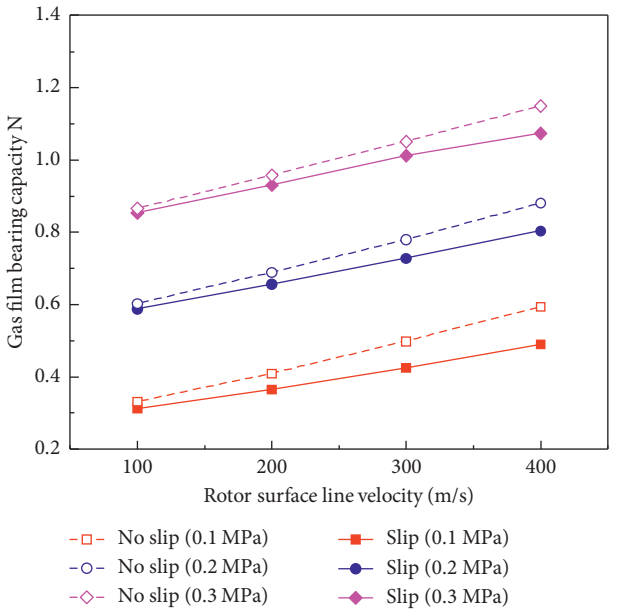

Figure 10: Gas film bearing capacity under different upstream and downstream pressure difference and speed conditions at temperature of 500°C.

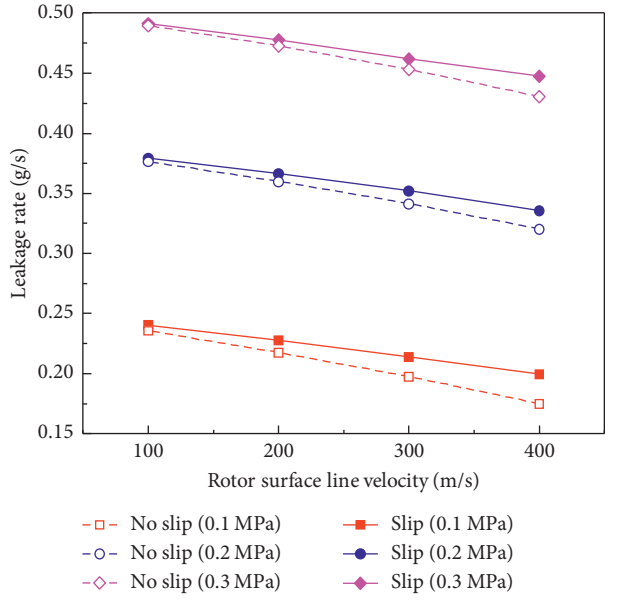

Figure 11: Leakage rate under different upstream and downstream pressure and speed conditions at temperature of 500°C.

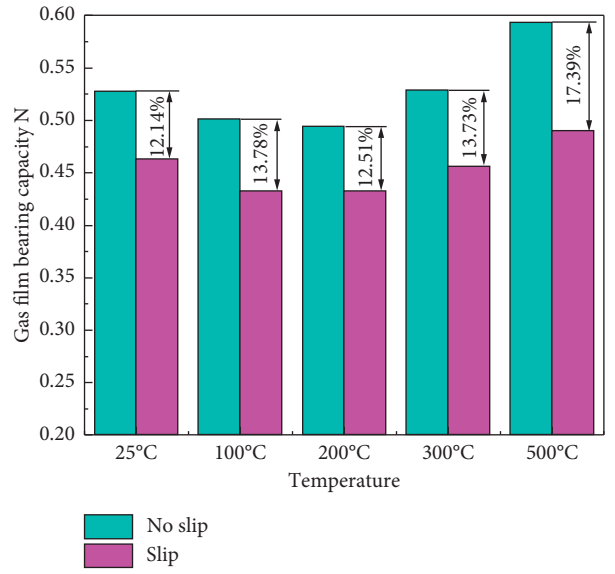

Figure 12: Gas film bearing capacity under different temperatures (ΔP = 0.1 MPa, v = 400 m/s).

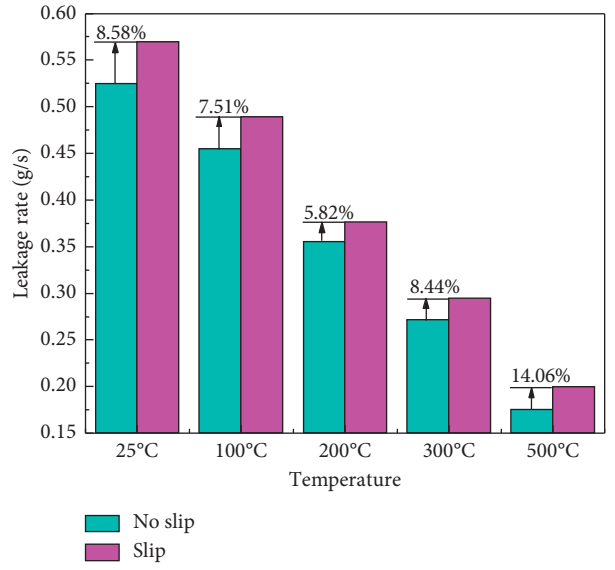

Figure 13: Leakage rate at different temperatures (ΔP = 0.1 MPa, v = 400 m/s).

analysis in Figures 12 and 13 show that, with the increasing influence of temperature on wall slip, the impact of wall slip effect needs to be considered when designing finger seal under high temperature application conditions, in order to design more accurate finger seal performance.

In order to further analyze the effect of thermal effect and boundary slip on the sealing properties of finger, the displacement calculation results of the inner surface of finger boots are given as shown in Figure 14. Considering the slip effect of the wall surface, the temperature has a consistent trend of influence on the leakage gap of the finger seal. With the increase of temperature, the deformation of the finger seal boot shows the trend of first decreasing and then increasing. However, considering the boundary slip, the deformation value of the finger seal boots under the same temperature conditions is greatly reduced, which also shows that it is necessary to consider the impact of wall slip. At the same time, the results show that 200°C is a turning point in the trend of change. When the temperature changes between 25°C and 200°C, as the temperature increases, it is affected by the thermal deformation effect, and the leakage gap of the finger seal appears to decrease.

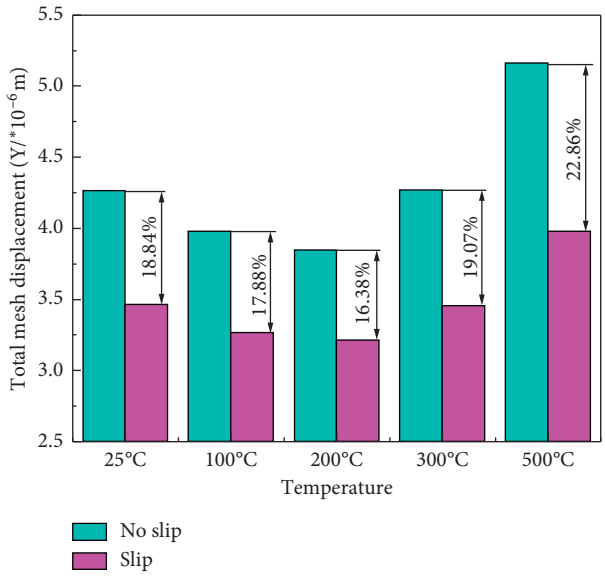

Figure 14: Y-direction displacement under different temperature conditions ($\Delta P = 0.1$ MPa, $v = 400$ m/s).

6. Conclusions

In this paper, the flow field model of hydrodynamic pressure finger seal gap is established based on the theory of microflow, and the slip effect of fluid seal is analyzed by CFX simulation; the key conclusions are summarized as follows.

(1) The hydrodynamic pressure finger seal leakage channel has microscale leakage flow characteristics. When the pressure difference is 0.1 MPa, the rotor line speed is 400 m/s, and the ambient temperature is 500°C and the slip rate has reached 27.28%. Therefore, it is significant to consider the impact of the wall slip effect in the design of hydrodynamic pressure finger seal under high-speed conditions.

(2) After considering the slip effect of the wall surface, the bearing capacity of the film decreases under the same working conditions, and the decrease is more obvious with the increase of the rotating speed. Under the above conditions, the bearing capacity of the gas film decreases by 17.39% compared with that without considering the slip, but the reduction value decreases with the increase of the pressure difference between the upper and lower reaches of the seal. It is explained that when hydrodynamic pressure finger seal is applied to low-pressure difference and high speed, it is necessary to consider wall slip in performance design.

(3) Considering the wall slip effect, the leakage rate of hydrodynamic finger seal increases under the same working condition, and the increasing range is more obvious with the increase of rotating speed. Under the above conditions, the leakage rate increases by 14.06% compared with that without considering slip, which shows that the effect of wall slip in the design of hydrodynamic finger seal cannot be ignored, and it needs to be considered in the performance design.

Data Availability

The indispensable data used to support the findings of this study are included within the article. More detailed data are available from the corresponding author upon request.

Conflicts of Interest

The authors declare no conflicts of interest.

Acknowledgments

The author would like to thank the National Natural Science Foundation of China (no. 51305343), Science and Technology Achievements Transfer and Promotion Plan Project of Shaanxi Province in China (2018XNCG-G-11), and Shaanxi Provincial Department of Education Service Local Special (industrialization) plan project (19JC030).

References

[1] G. D. Chen, H. Su, and Y. C. Zhang, *Analysis and Design of Finger Seal*, Northwest University of Technology Press, Evanston, IL, USA, 2012.

[2] G. X. Li, *Design and Simulation Analysis of Dynamic Pressure Finger Seal*, Northwestern Polytechnical University, Xi'an, China, 2007.

[3] M. P. Proctor and I. R. Delgado, "Leakage and power loss test results for competing turbine engine seals," in *Proceedings of Volume 4: Turbo Expo 2004*, p. 11, January 2004.

[4] H. Marie, "Dynamic simulation of finger seal-rotor interaction using variable dynamic coefficients," in *Proceedings of 42nd AIAA/ASME/SAE/ASEE Joint Propulsion Conference & Exhibit*, Sacramento, CA, USA, July 2006.

[5] M. J. Braun, H. M. Pierson, and V. V. Kudriavtsev, "Finger seal solid modeling design and some solid/fluid interaction considerations," *Tribology Transactions*, vol. 46, no. 4, pp. 566–575, 2003.

[6] J. M. Temis, A. V. Selivanov, and I. J. Dzeva, "Finger seal design based on fluid-solid interaction model," in *Proceedings of ASME Turbo Expo 2013: Turbine Technical Conference and Exposition*, San Antonio, TX, USA, December 2013.

[7] D. P. Fleming, *Gas Seal Pad with Herringbone-Grooved Rotor—Stiffness and Load Capacity*, NASA Glenn Research Center, Cleveland, OH, USA, 2006.

[8] M. P. Proctor, A. Kumar, and I. R. Delgado, "High-speed, high-temperature finger seal test results," *Journal of Propulsion & Power*, vol. 20, no. 2, pp. 312–318, 2002.

[9] G. J. Li, J. H. Li, and G. D. Chen, "Analysis of leakage characteristics of dynamic pressure finger seal," *Science and Technology*, vol. 7, no. 13, pp. 3157–3159f, 2007.

[10] X. L. Ma, G. D. Chen, and Y. C. Zhang, "Equivalent dynamic analysis of hydrodynamic finger seal," *Mechanical Science and Technology*, vol. 27, no. 11, pp. 1356–1360, 2008.

[11] K. B. Du, Y. J. li, and S. F. Suo, "A rear baffle with microporous texture non-contact finger seal device," CN Patent 104864102A, 2015.

[12] H. Zhang, Q. Zheng, and G. Q. Yue, "Analysis of the effect of finger seal boot structure on aerodynamic performance," *Journal of Engineering Thermo Physics*, vol. 33, no. 12, pp. 2076–2079, 2012.

[13] X. Jia, Q. Zheng, Z. Tian, Y. Jiang, and H. Zhang, "Numerical investigations on lifting and flow performance of finger seal

with grooved pad," *Aerospace Science and Technology*, vol. 81, pp. 225–236, 2018.

[14] G. Q. Li, Q. Zhang, L. Guo, Q. P. Yu, G. Xu, and J. Q. Zhu, "Leakage and wear characteristics of finger seal in hot/cold state for aero-engine," *Tribology International*, vol. 127, pp. 209–218, 2018.

[15] H. Zhao, G. Chen, L. N. Wang, H. Su, and F. Lu, "Dynamic performance of a C/C composite finger seal in a tilting mode," *Chinese Journal of Aeronautics*, vol. 30, no. 4, pp. 1603–1614, 2017.

[16] Y. E. Wu and G. D. Chen, "Finger seal design based on hysteretic performance optimization," *Lubrication and Sealing*, no. 2, pp. 125-126, 2005.

[17] G. D. Chen, H. Su, and Y. H. Zhang, "Study on the variable scale structure of the axial layout of finger seal," *Journal of Aerodynamics*, vol. 18, no. 4, pp. 488–491, 2003.

[18] X. L. Ma and G. D. Chen, "Hydrodynamic finger seal dynamics and leakage analysis based on the equivalent model," *Journal of Aeronautics*, vol. 29, no. 5, pp. 1356–1363, 2008.

[19] Z. Y. Ling, J. N. Ding, and J. C. Yang, "Research status and influencing factors of microflow," *Journal of Jiangsu University (Natural Science Edition)*, vol. 23, no. 6, pp. 1–5, 2002.

[20] C. W. Wu, G. J. Ma, and P. Zhou, "Research progress on boundary slip of fluid flow," *Advances in Mechanics*, vol. 38, no. 3, pp. 265–282, 2008.

[21] B. Y. Cao, M. Chen, and Z. Y. Guo, "Molecular dynamics of nano-channel slip flow," *Journal of Engineering Thermophysics*, vol. 7, no. 24, pp. 670–672, 2003.

[22] H. Wang, Y. Z. Hu, and Y. Guo, "Molecular dynamics study on slip of ultrathin lubricating film interface," *Journal of Tsinghua University (Natural Science Edition)*, vol. 40, no. 4, pp. 107–110, 2000.

[23] D. Chen, Y. H. Bian, S. Zhou, and J. W. Fan, "Influence factor analysis for gas fluctuation of aerostatic guideway," *Journal of Mechanical Engineering*, vol. 50, no. 15, pp. 97–103, 2014.

[24] X.-D. Chen and X.-M. He, "The effect of the recess shape on performance analysis of the gas-lubricated bearing in optical lithography," *Tribology International*, vol. 39, no. 11, pp. 1336–1341, 2006.

[25] P. Margaret and R. D. Irebert, "Preliminary test results of a non-contacting finger seal on a herringbone grooved rotor," in *Proceedings of 44th AIAA/ASME/SAE/ASEE Joint Propulsion Conference & Exhibit*, Hartford, CT, USA, July 2008.